Type-II InSe/*g*-C₃N₄ Heterostructure as a High-Efficiency Oxygen Evolution Reaction Catalyst for Photoelectrochemical Water Splitting

C. He,[†] J. H. Zhang,[†] W. X. Zhang,[*,‡] and T. T. Li[†]

[†]State Key Laboratory for Mechanical Behavior of Materials, School of Materials Science and Engineering, Xi'an Jiaotong University, Xi'an 710049, China

[‡]School of Materials Science and Engineering, Chang'an University, Xi'an 710064, China

Ⓢ *Supporting Information*

ABSTRACT: We propose a conceptual design of InSe/*g*-C₃N₄ van der Waals heterostructure to achieve highly efficient and spontaneous water splitting. InSe/*g*-C₃N₄ possesses a direct band gap of 2.04 eV with type-II band alignment, which is beneficial to the separation of electrons and holes and exhibits proper valence and conduction-band positions for the redox reactions of H₂O. In addition, the adsorption of multiple water molecules and the changes of free energy on InSe/*g*-C₃N₄ have been calculated to understand the oxygen evolution reaction (OER) process of water splitting. The free energies of reaction on three sides are all downhill, and the values of ΔG reduce to about −0.406 eV, indicating that the OER of water splitting is a thermodynamically permissible reaction without the aid of any other substance. Therefore, the water-splitting reaction could be thermodynamically continued using InSe/*g*-C₃N₄ as a photocatalyst, which indicates that InSe/*g*-C₃N₄ is an excellent candidate for photocatalyst or photoelectronic applications.
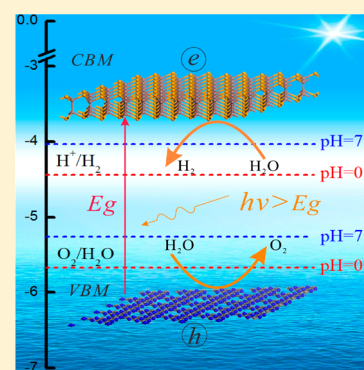
The development of renewable solar energy in the form of an effective storage chemical has been widely recognized as a promising and sustainable development strategy to meet the future global energy demand.[1,2] Taking advantage of a photocatalyst and solar energy, water splitting to generate oxygen and hydrogen is a low cost and a promising and appealing way to resolve the environmental issues and energy crisis.[3,4] On the basis of the definition of a photocatalyst, a desired water-splitting photocatalyst should have a narrow band gap for sunlight utilization, an excellent carrier separation for efficient surface activity, and suitable redox potentials for the sufficient driving force of the redox reaction, besides nontoxicity, economic viability, and photochemical stability.[5,6] Recently, great efforts have been made toward the development of photocatalysts, and the photocatalytic activity of a series of semiconductors has been extensively demonstrated, such as ZnO, WO₃, Bi₂WO₆, and CdS.[7−10] However, low absorption in visible light and high electron−hole recombination greatly limit the practical application of semiconductor photocatalysis. Therefore, it is a challenging task to search for active semiconductor photocatalysts that can split water directly under visible-light irradiation and improve its catalytic efficiency.

In recent years, polymeric graphite-like carbon nitride (*g*-C₃N₄), as a 2D layered semiconductor material with excellent chemical stability, nontoxicity, simple production procedure, low cost, and earth abundance, has been proved to be a promising candidate for water splitting.[11−13] Interestingly, the band gap of this metal-free material is 2.7 eV, which is suitable

to generate hydrogen and oxygen through water splitting under light irradiation.[14] However, the low quantum efficiency, which originates from the inefficient separation and transportation of the photogenerated electrons and holes for *g*-C₃N₄, still hinders the application of *g*-C₃N₄ as a water-splitting photocatalyst.[15,16] On the contrary, indium selenide (InSe) nanosheet exhibits a low formation energy with E_g of 1.4 eV and much larger carrier mobility compared with transition-metal dichalcogenides.[17,18] InSe nanosheet is analogous to that of black phosphorus and may be suitable for photocatalytic water splitting.[19] Moreover, the photodetectors based on few-layered InSe nanosheets also present a broadband from the visible to near-infrared region with a high photoresponsivity.[20] However, monolayer InSe presents indirect band-gap characteristics, which will prevent more applications in high-performance optoelectronic devices.[21] Also, the effort to extract the photocurrent has been hampered by the need to separate the electron and hole pairs created by the incoming photons.[22] To date, the construction of heterojunction structures is considered to be an effective way to modify the atomic and electronic structures of photocatalysts to accelerate the separation and transmission of electron holes.[23,24] van der Waals (vdW) heterostructures with different 2D ultrathin functional nanosheets (e.g., MoS₂/graphene and SnSe₂/WSe₂)

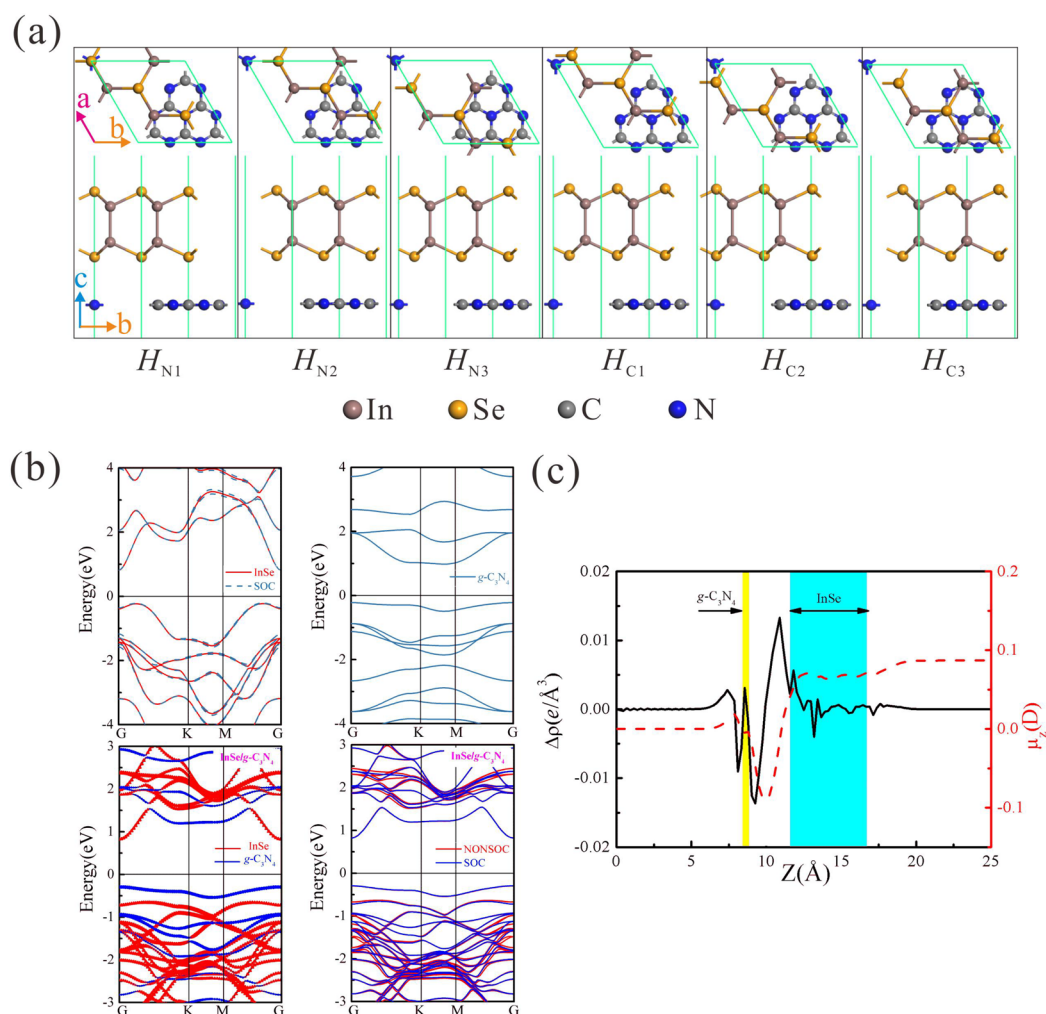**Figure 1.** (a) Top and side views of the three inequivalent stacking patterns of InSe/g-C₃N₄: H_{N1}, H_{N2}, H_{N3}, H_{C1}, H_{C2}, and H_{C3}. (b) Computed band structures of the monolayer InSe, monolayer g-C₃N₄, and InSe/g-C₃N₄, including the SOC and non-SOC band structures. (c) Planar average charge density difference (solid black) and interface dipole moment (red dashed) along the z direction for InSe/g-C₃N₄.

have been successfully applied to suppress the photoexcited electron−hole recombination in bulk materials in an attempt to simultaneously promote charge transfer.[25] To further extend the applications of the 2D InSe nanosheet, several researchers have worked on InSe-based vdW heterostructures, such as InSe/graphene and InSe/black phosphorus, so far.[26,27] Because of the similar properties between monolayered InSe and g-C₃N₄, we design and predict InSe/g-C₃N₄ vdW heterostructures for highly efficient visible-light photocatalysts that can effectively prevent the recombination of the photoinduced electrons and holes and eventually facilitate the charge separation.

In our study, we have systematically investigated the structural and electronic properties, the band alignment, as well as the water adsorption and decomposition of the InSe/g-C₃N₄ heterostructure by using first-principles calculation. A typical type-II band alignment forms between InSe and g-C₃N₄ monolayers, and both the valence band maximum (VBM) and the conduction band minimum (CBM) of InSe are lower than those of g-C₃N₄. Furthermore, the structural and thermodynamic performances during the oxygen evolution reaction (OER) of water spitting on three sides of the InSe/g-C₃N₄ heterostructure have been systematically studied. It is meaningful to find that the InSe/g-C₃N₄ heterostructure is an

excellent candidate for photocatalyst or photoelectronic applications, which provide theoretical guidance for applications in next-generation nanoelectronic devices.

The first-principles calculations were performed by the Vienna ab initio simulation package (VASP) with the projector-augmented wave (PAW), based on the density functional theory (DFT).[28,29] The Perdew−Burke−Ernzerhof (PBE) scheme within the generalized gradient approximation (GGA) was used to treat the exchange-correlation interaction of electrons.[30,31] Considering the underestimation of the PBE functional on the band gap of the semiconductor, the HSE06 hybrid functional was also applied for more accurate electronic structure and optical properties calculations.[32] Because the weak interactions were not well described by the standard PBE functional, the empirical correction scheme of the DFT-D2 (D stands for dispersion) approach within the Grimme scheme was adopted for the nontrivial vdW interaction.[33] A kinetic energy cutoff was set to be 600 eV for the plane-wave expansion. The convergence tolerances for energy, force, and maximum displacement on each atom during structural relaxation were set to 10^{-4} eV, 0.01 eV/Å, and 0.005 Å, respectively. A Monkhorst−Pack k-point mesh of $7 \times 7 \times 1$ was respectively used to calculate the properties of all of the studies in the 2D Brillouin zone. To avoid the interaction

between neighboring layers and its periodic impact, a vacuum spacing of 25 Å was added along the direction perpendicular to 2D nanosheet. Moreover, a well-known fact is that relativistic effects (of which spin−orbit is a part) grow approximately as Z^2, where Z is the atomic number, and they are definitely important for compounds of elements in the fifth period. Spin−orbit coupling (SOC) is included in our calculation to examine the influence of SOC on splitting of the electronic bands.[22]

The InSe/g-C$_3$N$_4$ heterostructure is achieved by InSe and g-C$_3$N$_4$ monolayers stacked in the vertical direction with consideration of vdW interactions.[34,35] The calculated lattice parameters of the InSe ($a = b = 4.07$ Å) and g-C$_3$N$_4$ ($a = b = 7.06$ Å) monolayers are in good agreement with experimental and other theoretical calculations.[36,37] A $\sqrt{3} \times \sqrt{3}$ InSe supercell and a 1×1 g-C$_3$N$_4$ supercell are adopted to construct the InSe/g-C$_3$N$_4$ heterostructure to minimize the lattice mismatch to 0.78%. In Figure 1a, according to the relative position of the InSe and g-C$_3$N$_4$ monolayers, we have constructed six stacking patterns: C atoms of g-C$_3$N$_4$ locate in the hexagonal ring center of InSe (labeled as H_{C1}, H_{C2}, and H_{C3}), and N atoms of g-C$_3$N$_4$ locate in the hexagonal ring center of InSe (labeled as H_{N1}, H_{N2}, and H_{N3}). To check the stability of the heterostructure and quantitatively characterize the interlayer interaction intensity, the binding energy (E_b) per unit cell is calculated by the following formula

$$E_b = E_{InSe/g\text{-}C_3N_4} - E_{InSe} - E_{g\text{-}C_3N_4} \qquad (1)$$

where $E_{InSe/g\text{-}C_3N_4}$, E_{InSe}, and $E_{g\text{-}C_3N_4}$ represent the total energies of the InSe/g-C$_3$N$_4$ heterostructure, the isolated InSe, and the g-C$_3$N$_4$ monolayer, respectively. According to the definition, the negative value of E_b indicates that the heterostructure system is energetically stable. The corresponding parameters of the six stacking patterns after the geometric optimization are listed in Table 1, where the structures of H_{C1},

Table 1. Summary of the Structural and Electronic Properties of InSe/g-C$_3$N$_4$ for Different Stacking Patterns[a]

type	InSe/g-C$_3$N$_4$					
stacking patterns	H_{N1}	H_{N2}	H_{N3}	H_{C1}	H_{C2}	H_{C3}
d_0 (Å)	2.604	2.925	3.025	2.722	2.796	2.625
E_b (eV)	−2.315	−2.188	−2.187	−2.313	−2.311	−2.312
E_g (eV)	1.581	1.826	1.729	1.678	1.566	1.673

[a]d_0, E_b, and E_g are the values of lattice parameters, the binding energy, and the band gap.

H_{C2}, and H_{C3} are optimized to H_{N1} due to the instability of the three structures. It can be seen that pattern H_{N1} has the smallest binding energy of −2.315 eV with the interlayer distance of 2.604 Å, which indicates that H_{N1} should be chosen as the heterostructure's stacking model in the following calculations.

The band structures of monolayer g-C$_3$N$_4$, monolayer InSe, and InSe/g-C$_3$N$_4$ heterostructure with and without SOC are shown in Figure 1b. The SOC causes an additional slight splitting of the bands with a value of <0.1 eV. Hence, it will not be discussed in the following studies. It can be seen that both InSe and g-C$_3$N$_4$ monolayers are indirect semiconductors, with E_g values of 1.372 eV (2.29 eV) and 1.182 eV (2.63 eV) at the GGA-PBE (HSE06) level, respectively. After contacting, the

InSe/g-C$_3$N$_4$ heterostructure has a direct band gap, where CBM and VBM are both located in the G (Γ) point. Because of the influence of vdW interactions between InSe and g-C$_3$N$_4$ monolayers, E_g of the InSe/g-C$_3$N$_4$ heterostructure is reduced to 2.06 eV at the HSE06 level, which is less than E_g of InSe and g-C$_3$N$_4$ monolayers. VBM is mainly contributed by g-C$_3$N$_4$, whereas CBM is mainly provided by InSe, which indicates that InSe/g-C$_3$N$_4$ is a typical type-II vdW heterostructure, and the excited electrons and holes are, respectively, localized in InSe and g-C$_3$N$_4$ layers, facilitating the effective separation of the photogenerated holes and electrons. To gain more insights into the electronic structures of the InSe/g-C$_3$N$_4$ heterostructure, the electron density of states (DOS) and partial density of states (PDOS) are plotted in Figure S1 and are discussed in Supporting Information.

To further study the interaction mechanism of InSe/g-C$_3$N$_4$, the planar average charge density difference $\Delta\rho(z)$ is calculated, which is given as

$$\Delta\rho(z) = \rho(z)_{InSe/g\text{-}C_3N_4} - \rho(z)_{InSe} - \rho(z)_{g\text{-}C_3N_4} \qquad (2)$$

where $\rho(z)_{InSe/g\text{-}C_3N_4}$, $\rho(z)_{InSe}$, and $\rho(z)_{g\text{-}C_3N_4}$ are the planar average charge densities of the combined InSe/g-C$_3$N$_4$ system, the InSe monolayer, and the g-C$_3$N$_4$ monolayer, respectively. In Figure 1c, vertical bars indicate the positions of InSe and g-C$_3$N$_4$ monolayers. Here negative values of $\Delta\rho(z)$ areas highlight the regions of charge accumulation, whereas positive values of $\Delta\rho(z)$ areas mark the regions of charge depletion. The change at the interfaces indicates that the electrons transfer from g-C$_3$N$_4$ to the InSe side across the interface, and thereby the holes remain in the g-C$_3$N$_4$ side. To further understand the interfacial electronic properties, we have calculated the interface dipole moment $\mu(z)$ as follows

$$\mu(z) = \int z\Delta\rho(z)\,dz \qquad (3)$$

A dipole moment $\mu(z)$ of +0.086 D is found, thus confirming the formation of a heterostructure-induced interface dipole, where a positive value of $\mu(z)$ suggests an inward pointing dipole,[38] that is, from the InSe layer (with electrons) to the g-C$_3$N$_4$ layer (with holes). Furthermore, we have also checked the direction of the interface dipole by comparing the electrostatic potentials of the interface and those of isolated InSe and g-C$_3$N$_4$ (vacuum level shift). It is found that the work function of monolayer g-C$_3$N$_4$ ($\Phi = 4.34$ eV) is smaller than that of monolayer InSe ($\Phi = 5.38$ eV), as seen in Figure S2. If the work functions of the two materials forming the heterojunction are different, then the interface dipole will be present, which directs toward to the layer with a smaller work function.[39] Therefore, the direction of the interface dipole of the InSe/g-C$_3$N$_4$ heterostructure is directed toward the g-C$_3$N$_4$ layer, which is consistent with the above results of $\mu(z)$.

Finally, we explore whether the InSe/g-C$_3$N$_4$ heterostructure could be a better candidate in photocatalytic reactions, especially water splitting. It should be noted that the water redox potential also depends on the pH value.[40,41] The standard oxidation potential of O$_2$/H$_2$O can be calculated by $E_{O_2/H_2O} = -5.67$ eV + pH × 0.059 eV, and the reduction potential for H$^+$/H$_2$ is determined by $E_{H^+/H_2} = -4.44$ eV + pH × 0.059 eV. The unique feature of chalcogenides is their high stability in an acidic environment, especially in combination with other transition metals.[42] Hence, the redox potential in a
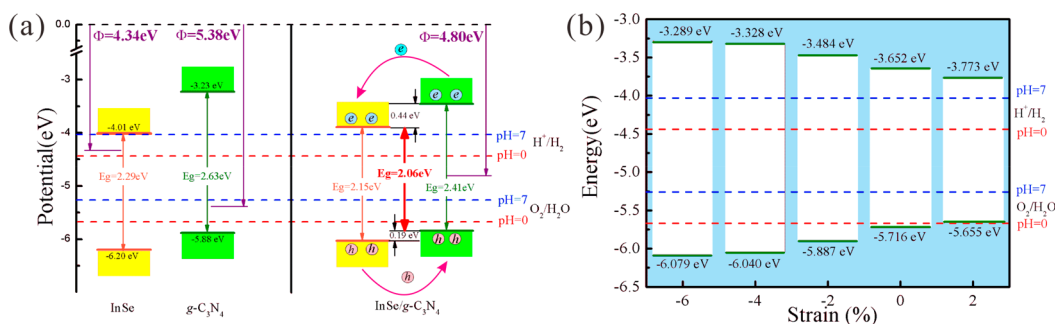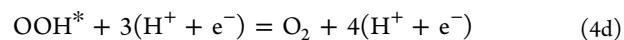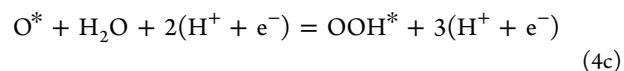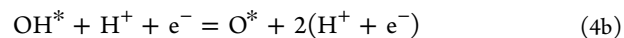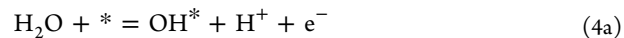
Figure 2. (a) Band-edge positions of the free-standing InSe and g-C$_3$N$_4$ monolayers as well as that of the InSe/g-C$_3$N$_4$. (b) Calculated band alignment of the InSe/g-C$_3$N$_4$ at the HSE06 level as a function of biaxial strain.

neutral environment (pH 7) is also studied, as seen by the blue dotted lines of Figure 2a. From the VBM and the CBM of the InSe and g-C$_3$N$_4$ monolayers presented, E_g of InSe spans from −6.20 to −4.01 eV, whereas E_g of g-C$_3$N$_4$ spans from −5.88 to −3.23 eV. Both InSe and g-C$_3$N$_4$ monolayers satisfy the conditions of photocatalytic water splitting. However, the calculated band-edge positions of InSe and g-C$_3$N$_4$ are their potentials before contact. After g-C$_3$N$_4$ monolayer comes into contact with InSe monolayer, the electronic properties of the constituents could be changed. Because the work function of g-C$_3$N$_4$ (4.34 eV) is lower than that of InSe (5.67 eV), the electrons flow from g-C$_3$N$_4$ to InSe to align the Fermi energy, thus causing the change of relative band-edge position, as shown in Figure 2a. The VBM band is mainly composed of g-C$_3$N$_4$ states with a value of −5.84 eV, which is more negative than the oxidation potential (−5.67 eV at pH 0 and −5.26 eV at pH 7) of H$_2$O/O$_2$ for water splitting, whereas InSe contributes to the bottom part of the lowest conduction band (CB) with a value of −3.90 eV, which is less negative than the oxidation potential (−4.44 eV at pH 0 and −4.03 eV at pH 7) of H$^+$/H$_2$. Consequently, the valence band offset (VBO) between InSe and g-C$_3$N$_4$ is ∼0.2 eV, whereas the conduction band offset (CBO) between them is ∼1.1 eV. In the photocatalysis process, the electrons could be photogenerated from the CB of monolayer InSe when the InSe/g-C$_3$N$_4$ heterostructure is illuminated by incident light. The existence of CBO induces the photogenerated electrons in the CB of g-C$_3$N$_4$ to inject into the CB of InSe. Simultaneously, the existence of the VBO induces the photogenerated holes in the valence band (VB) of InSe to drift to the VB of g-C$_3$N$_4$, which results in the separation of the electron and the hole on InSe and g-C$_3$N$_4$ monolayers, respectively. The separation in space could restrain the recombination of electron−hole pairs and prolong the lifetime of photogenerated carriers, which improves the photocatalytic bands of monolayer InSe, and the oxidation of water on the VBs of monolayer g-C$_3$N$_4$ could be conducted.

Strain engineering has been known as an effective method in controlling the electronic, transport, and optical properties of semiconductors for decades.[43] This tool is particularly useful in engineering 1D and 2D crystals because these reduced-dimensional structures can sustain much larger strains than the corresponding bulk crystals. Therefore, we explore how strain affects the band edges and the band gap of the InSe/g-C$_3$N$_4$ heterostructure. The in-plane strain has been applied by biaxially stretching the hexagonal cell, and the biaxial strain is defined as $\varepsilon = \Delta a/a_0$, where a_0 is the lattice constant of the InSe/g-C$_3$N$_4$ heterostructure in its equilibrium state and Δa is

the difference between the strained lattice constant and the unstrained lattice constant of the InSe/g-C$_3$N$_4$ heterostructure. Our results in Figure 2b suggest that the InSe/g-C$_3$N$_4$ heterostructure could ensure a suitable band alignment when applying a biaxial strain from −6 to +2% without damaging its structure. The position of VBM (CBM) increases (decreases) linearly when the strain changes from −6 to +2%. The band edges of all of the compressed strain systems are proper for initializing the photocatalytic redox reactions of water, whereas the reduction reaction becomes energetically impossible for the stretched strain systems. Such a desirable band-edge alignment of the InSe/g-C$_3$N$_4$ heterostructure indicates a strong compressed strain tolerance of the photocatalytic water-splitting abilities.

In addition, the adsorption and reaction of H$_2$O on the surface or in the interface of InSe/g-C$_3$N$_4$ heterostructure is another important parameter to characterize its activity in the photocatalytic water-splitting application. Figure S3 shows the most stable adsorption structures of H$_2$O on three sides of InSe/g-C$_3$N$_4$ with a 2 × 2 supercell. After the adsorption of the water molecule on the InSe/g-C$_3$N$_4$ heterostructure is studied, it is used as the basis to investigate the catalytic decomposition of the water molecule. Relative to the total reaction of the water molecule, there are two half-reactions: OER in anode: H$_2$O → 1/2O$_2$ + 2H$^+$ + 2e$^-$; hydrogen evolution reaction (HER) in cathode: 2H$^+$ + 2e$^-$ → H$_2$. However, OER is recognized as a much more complicated process that involves four-electron transfer. In our model, we assume that the OER proceeds through one-electron transfer steps according to the following pathway

$$H_2O + * = OH^* + H^+ + e^- \tag{4a}$$

$$OH^* + H^+ + e^- = O^* + 2(H^+ + e^-) \tag{4b}$$

$$O^* + H_2O + 2(H^+ + e^-) = OOH^* + 3(H^+ + e^-) \tag{4c}$$

$$OOH^* + 3(H^+ + e^-) = O_2 + 4(H^+ + e^-) \tag{4d}$$

where * indicates the active site on the surface of the substrate. The absorption states of OH*, O*, and OOH* intermediates on catalysts are particularly important to understand the water-splitting process. Detailed configurations of them are shown in Figure S3 and Table S1, and the corresponding adsorption energies are calculated. The change of free energy (ΔG) is calculated using the following equation

$$\Delta G = \Delta E + \Delta ZPE - T\Delta S - \Delta G_U - \Delta G_{pH} \tag{5}$$

where G, E, ZPE, and TS are the free energy, the total energy from the DFT calculation, the zero-point energy, and the entropic contribution (T is set to be 298.15 K), respectively. ZPE could be derived after the frequency calculation by

$$ZPE = 1/2 \sum h\nu_i \qquad (6)$$

The TS values of adsorbed species are calculated after the vibrational frequencies are obtained

$$TS_\nu = k_B T \left[\sum_K \ln\left(\frac{1}{1 - e^{-h\nu/k_B T}}\right) + \sum_K \frac{h\nu}{k_B T}\left(\frac{1}{e^{h\nu/k_B T} - 1}\right) + 1\right] \qquad (7)$$

$\Delta G_U = -eU$ represents the effect of a potential bias on all states involving one electron in the electrode, where e is the elementary positive charge and U is the potential measured against the normal hydrogen electrode. When pH does not equal 0, the G values of H$^+$ ions are corrected by $\Delta G_{pH} = -k_B T \ln 10 \times pH$. Here pH 0 and pH 7 are considered. Using the standard hydrogen electrode (SHE) as the reference, the reaction G of $1/2 H_2 \rightarrow H^+ + e^{-1}$ is zero at pH 0, p = 1 bar, and T = 298.15 K. Therefore, the G of $(H^+ + e^-)$ is equal to the G of $1/2\ H_2$ under standard conditions.

The calculated free-energy changes of the OER process on the InSe/g-C$_3$N$_4$ heterostructure for the proposed four reaction steps at the equilibrium potential of 1.23 V (pH 0) are plotted in Figure 3 and are listed in Table S2. Clearly, the
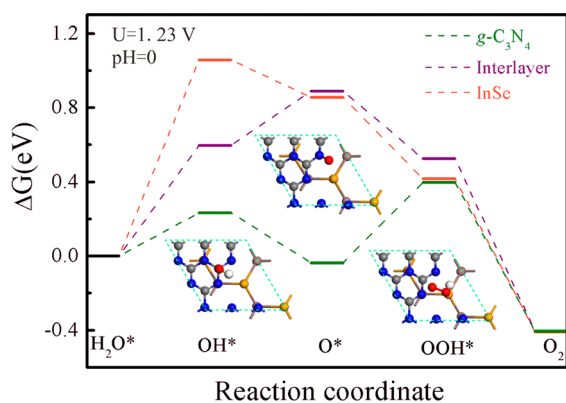

Figure 3. Free-energy (ΔG, eV) profiles of the OER (pH 0, U = 1.23 V) on the InSe surface, the g-C$_3$N$_4$ surface, and the interlayer of InSe/g-C$_3$N$_4$. The surface structures of the g-C$_3$N$_4$ surface in different stages are shown in the inset.

rate-determining steps are the step of O* to OOH*, with the largest ΔG of 0.433 eV on the g-C$_3$N$_4$ side, and the

dissociation of H$_2$O to OH*, with the largest ΔG values of 1.057 and 0.596 eV on the InSe side and the interface of InSe/g-C$_3$N$_4$, separately. Increasing ΔG on three sides for the step of H$_2$O to OH* shows that the InSe/g-C$_3$N$_4$ catalyst exhibits a high activated water adsorption energy on the three sides, which hinders the dissociation of water to OH* intermediates and leads to sluggish OER kinetics. For the dissociation of OH* to O*, the G of the reaction on the g-C$_3$N$_4$ (InSe) side decreases from 0.232 (1.057) eV to −0.036 (0.855) eV but increases on the interface of InSe/g-C$_3$N$_4$ from 0.596 to 0.890 eV. Next, O* reacts with another H$_2$O molecule to generate the OOH* group. In this step, ΔG is positive for the g-C$_3$N$_4$ side, with a value of 0.434 eV, and negative for another two sides, with values of −0.438 and −0.365 eV. For the final step, the OOH* group dehydrogenates and converts to O$_2$. The G values of the reactions on the three sides are all downhill, and the values of ΔG reduce to about −0.406 eV, indicating that the OOH* peroxo species easily breaks down to generate oxygen. It can be shown that the OER process on the g-C$_3$N$_4$ side is more energetically favorable than that on the another two sides and leads to a reduced energy barrier of the initial water dissociation step and subsequent dehydrogenation of OH*. Therefore, we mainly discuss the corresponding ΔG of the OER on the g-C$_3$N$_4$ side with different potentials under pH 0 and 7.

The difference between the photodehydration reduction potential and the potential corresponding to the InSe/g-C$_3$N$_4$ VB is considered to be the driving force for photooxidation of water under illumination conditions. The potential of the VB edge (U_{VB}) of the InSe/g-C$_3$N$_4$ heterostructure relative to the SHE is U = ~1.40 V at pH 0 and U = ~1.81 V at pH 7. Figure 4 shows the corresponding ΔG at external potential (U = 0 V), equilibrium potential (U = 1.23 V), and corresponding potential of the VB under the extreme conditions of pH 0 and 7. It is shown that at U = 0 V, the G for every step increases at pH 0 and 7, which means that the reactions need to overcome a large energy barrier (ΔG = 4.514 eV at pH 0 and ΔG = 4.099 eV at pH 7). At the equilibrium potential U = 1.23 V at pH 0 and 7, the free energies of the dehydrogenation steps of OH* and OOH* decrease, but for the other two steps, they still increase. At an operating potential of 1.40 V (pH 0), ΔG for the dehydrogenation of H$_2$O and generation of OOH* turns out to be less positive, and ΔG for the dissociation of OH* and OOH* is more negative. This indicates that the OER becomes easier under the driving force of the InSe/g-C$_3$N$_4$ VB edge. When an external potential U = 1.81 V is applied at pH 7, the G of all steps involved in the reaction is reduced, and the reaction is thermodynamically sustainable.
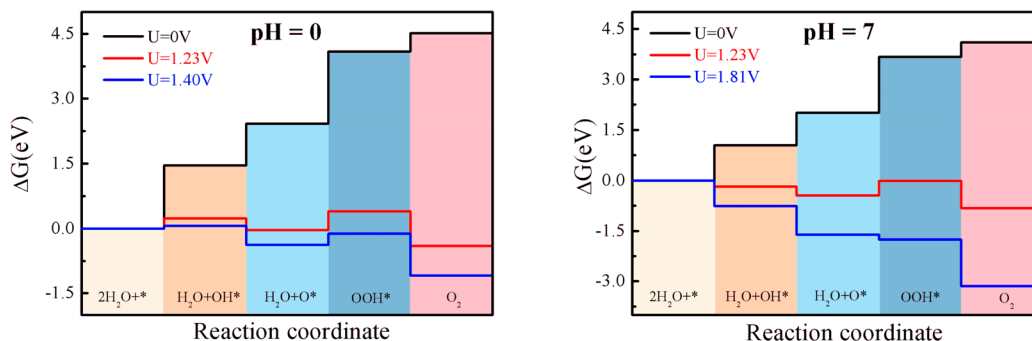

Figure 4. Free energies of the intermediates on g-C$_3$N$_4$ surface at pH 0 and 7 at different potentials.

Therefore, by using the InSe/g-C$_3$N$_4$ heterostructure as a photoelectrode, the photocatalytic decomposition of water is a thermodynamically permissible reaction without the aid of any other substance.

CONCLUSIONS

We have explored the potential of the InSe/g-C$_3$N$_4$ heterostructure for oxygen evolution electrocatalysis of water splitting by DFT calculations. The InSe/g-C$_3$N$_4$ heterostructure is a typical type-II semiconductor with a direct band gap of 2.04 eV, where CBMs and VBMs are separately contributed by InSe and g-C$_3$N$_4$, respectively. Furthermore, the calculated E_{ads} values for H$_2$O-InSe/g-C$_3$N$_4$, InSe/g-C$_3$N$_4$−H$_2$O, and InSe/H$_2$O/g-C$_3$N$_4$ are −0.376, −0.778, and −0.991 eV, respectively, which are beneficial for water-splitting reactions. The G values of the reactions on three sides are all downhill, and the values of ΔG reduce to about −0.406 eV. When an external potential U = 1.81 V is applied at pH 7, the driving force provided by the InSe/g-C$_3$N$_4$ VB could ensure the negative free energy of all steps, which indicates that the OER of water splitting is a thermodynamically permissible reaction without the aid of any other substance. These studies suggest that the InSe/g-C$_3$N$_4$ heterostructure could be used as a high-performance OER electrocatalyst.

ASSOCIATED CONTENT

Ⓢ Supporting Information

The Supporting Information is available free of charge on the ACS Publications website at DOI: 10.1021/acs.jpclett.9b00909.

Calculated DOSs and electrostatic potentials for InSe monolayer, g-C$_3$N$_4$ monolayer, and InSe/g-C$_3$N$_4$; stable adsorption structures of H$_2$O, OH*, O*, and OOH*; and specific data of ΔG calculation (PDF)

AUTHOR INFORMATION

Corresponding Author

*E-mail: wxzhang@chd.edu.cn.

ORCID Ⓘ

W. X. Zhang: 0000-0002-9327-5761

Notes

The authors declare no competing financial interest.

ACKNOWLEDGMENTS

REFERENCES

(1) Huang, X. J.; Meng, Q. B.; Chen, H.; Du, X. L.; Chen, L. Q. Renewable Energy Conversion, Storage, and Efficient Utilization. *Science* **2018**, *360*, 47−51.

(2) Zhou, Y.; Liu, Y. S. Help Relieve Poverty with Solar Power. *Nature* **2018**, *560*, 29−29.

(3) Ye, S.; Wang, R.; Wu, M. Z.; Yuan, Y. P. A Review on g-C$_3$N$_4$ for Photocatalytic Water Splitting and CO$_2$ Reduction. *Appl. Surf. Sci.* **2015**, *358*, 15−27.

(4) Zhang, R. Q.; Zhang, L. L.; Zheng, Q. J.; Gao, P. F.; Zhao, J.; Yang, J. L. Direct Z-Scheme Water Splitting Photocatalyst Based on Two-Dimensional Van Der Waals Heterostructures. *J. Phys. Chem. Lett.* **2018**, *9*, 5419−5424.

(5) Hisatomi, T.; Kubota, J.; Domen, K. Recent Advances in Semiconductors for Photocatalytic and Photoelectrochemical Water Splitting. *Chem. Soc. Rev.* **2014**, *43*, 7520−7535.

(6) Shavorskiy, A.; Ye, X. F.; Karslioglu, O.; Poletayev, A. D.; Hartl, M.; Zegkinoglou, I.; Trotochaud, L.; Nemsak, S.; Schneider, C. M.; Crumlin, E. J.; et al. Direct Mapping of Band Positions in Doped and Undoped Hematite during Photoelectrochemical Water Splitting. *J. Phys. Chem. Lett.* **2017**, *8*, 5579−5586.

(7) Etacheri, V.; Roshan, R.; Kumar, V. Mg-Doped ZnO Nanoparticles for Efficient Sunlight-Driven Photocatalysis. *ACS Appl. Mater. Interfaces* **2012**, *4*, 2717−2725.

(8) Szilagyi, I. M.; Forizs, B.; Rosseler, O.; Szegedi, A.; Nemeth, P.; Kiraly, P.; Tarkanyi, G.; Vajna, B.; Varga-Josepovits, K.; Laszlo, K.; et al. WO$_3$ Photocatalysts: Influence of Structure and Composition. *J. Catal.* **2012**, *294*, 119−127.

(9) Tian, J.; Sang, Y. H.; Yu, G. W.; Jiang, H. D.; Mu, X. N.; Liu, H. A Bi$_2$WO$_6$-Based Hybrid Photocatalyst with Broad Spectrum Photocatalytic Properties under UV, Visible, and Near-Infrared Irradiation. *Adv. Mater.* **2013**, *25*, 5075−5080.

(10) Hu, Y.; Gao, X. H.; Yu, L.; Wang, Y. R.; Ning, J. Q.; Xu, S. J.; Lou, X. W. Carbon-Coated CdS Petalous Nanostructures with Enhanced Photostability and Photocatalytic Activity. *Angew. Chem., Int. Ed.* **2013**, *52*, 5636−5639.

(11) Wen, J. Q.; Xie, J.; Chen, X. B.; Li, X. A Review on g-C$_3$N$_4$-based Photocatalysts. *Appl. Surf. Sci.* **2017**, *391*, 72−123.

(12) Cao, S. W.; Yu, J. G. g-C$_3$N$_4$-Based Photocatalysts for Hydrogen Generation. *J. Phys. Chem. Lett.* **2014**, *5*, 2101−2107.

(13) Li, T. T.; He, C.; Zhang, W. X. A Novel Porous C$_4$N$_4$ Monolayer as a Potential Anchoring Material for Lithium−sulfur Battery Design. *J. Mater. Chem. A* **2019**, *7*, 4134−4144.

(14) Safaei, J.; Mohamed, N. A.; Mohamad Noh, M. F.; Soh, M. F.; Ludin, N. A.; Ibrahim, M. A.; Roslam Wan Isahak, W. N.; Mat Teridi, M. A. Graphitic Carbon Nitride (g-C$_3$N$_4$) Electrodes for Energy Conversion and Storage: a Review on Photoelectrochemical Water Splitting, Solar Cells and Supercapacitors. *J. Mater. Chem. A* **2018**, *6*, 22346−22380.

(15) Liu, J.; Liu, Y.; Liu, N. Y.; Han, Y. Z.; Zhang, X.; Huang, H.; Lifshitz, Y.; Lee, S. T.; Zhong, J.; Kang, Z. H. Metal-free Efficient Photocatalyst for Stable Visible Water Splitting via a Two-electron Pathway. *Science* **2015**, *347*, 970−974.

(16) Lin, S.; Ye, X. X.; Gao, X. M.; Huang, J. Mechanistic Insight into the Water Photooxidation on Pure and Sulfur-doped g-C$_3$N$_4$ Photocatalysts from DFT Calculations with Dispersion Corrections. *J. Mol. Catal. A: Chem.* **2015**, *406*, 137−144.

(17) Shen, T.; Ren, J. C.; Liu, X. Y.; Li, S.; Liu, W. van der Waals Stacking Induced Transition from Schottky to Ohmic Contacts: 2D Metals on Multilayer InSe. *J. Am. Chem. Soc.* **2019**, *141*, 3110−3115.

(18) Liu, X. Y.; Ren, J. C.; Zhang, S. F.; Fuentes-Cabrera, M.; Li, S.; Liu, W. Ultrahigh Conductivity in Two-Dimensional InSe via Remote Doping at Room Temperature. *J. Phys. Chem. Lett.* **2018**, *9*, 3897−3903.

(19) Li, L. K.; Yang, F. Y.; Ye, G. J.; Zhang, Z. C.; Zhu, Z. W.; Lou, W. K.; Zhou, X. Y.; Li, L.; Watanabe, K.; Taniguchi, T.; et al. Quantum Hall Effect in Black Phosphorus Two-dimensional Electron System. *Nat. Nanotechnol.* **2016**, *11*, 592−596.

(20) Lei, S. D.; Wen, F. F.; Ge, L. H.; Najmaei, S.; George, A.; Gong, Y. J.; Gao, W. L.; Jin, Z. H.; Li, B.; Lou, J.; et al. An Atomically Layered InSe Avalanche Photodetector. *Nano Lett.* **2015**, *15*, 3048−3055.

(21) Shang, J. M.; Pan, L. F.; Wang, X. T.; Li, J. B.; Deng, H. X.; Wei, Z. M. Tunable Electronic and Optical Properties of InSe/InTe van der Waals Heterostructures toward Optoelectronic Applications. *J. Mater. Chem. C* **2018**, *6*, 7201−7206.

(22) Zhang, J.; Lang, X. Y.; Zhu, Y. F.; Jiang, Q. Strain Tuned InSe/MoS₂ Bilayer van der Waals Heterostructures for Photovoltaics or Photocatalysis. *Phys. Chem. Chem. Phys.* **2018**, *20*, 17574−17582.

(23) Che, W.; Cheng, W. R.; Yao, T.; Tang, F. M.; Liu, W.; Su, H.; Huang, Y. Y.; Liu, Q. H.; Liu, J. K.; Hu, F. C.; et al. Fast Photoelectron Transfer in (C-ring)-C₃N₄ Plane Heterostructural Nanosheets for Overall Water Splitting. *J. Am. Chem. Soc.* **2017**, *139*, 3021−3026.

(24) He, C.; Zhang, J. H.; Zhang, W. X.; Li, T. T. GeSe/BP van der Waals Heterostructures as Promising Anode Materials for Potassium-Ion Batteries. *J. Phys. Chem. C* **2019**, *123*, 5157−5163.

(25) Deng, D. H.; Novoselov, K. S.; Fu, Q.; Zheng, N. F.; Tian, Z. Q.; Bao, X. H. Catalysis with Two-dimensional Materials and Their Heterostructures. *Nat. Nanotechnol.* **2016**, *11*, 218−230.

(26) Luo, W.; Cao, Y.; Hu, P.; Cai, K.; Feng, Q.; Yan, F.; Yan, T.; Zhang, X.; Wang, K. Gate Tuning of High-Performance InSe-Based Photodetectors Using Graphene Electrodes. *Adv. Opt. Mater.* **2015**, *3*, 1418−1423.

(27) Padilha, J. E.; Miwa, R. H.; da Silva, A. J. R.; Fazzio, A. Two-dimensional van der Waals p-n Junction of InSe/phosphorene. *Phys. Rev. B: Condens. Matter Mater. Phys.* **2017**, *95*, 6.

(28) Sham, L. J.; Kohn, W. One-Particle Properties of an Inhomogeneous Interacting Electron Gas. *Phys. Rev.* **1966**, *145*, 561.

(29) Kresse, G.; Furthmuller, J. Efficient Iterative Schemes for ab Initio Total-energy Calculations Using a Plane-wave Basis Set. *Phys. Rev. B: Condens. Matter Mater. Phys.* **1996**, *54*, 11169−11186.

(30) Perdew, J. P.; Burke, K.; Ernzerhof, M. Generalized Gradient Approximation Made Simple. *Phys. Rev. Lett.* **1996**, *77*, 3865−3868.

(31) Su, G. R.; Yang, S.; Li, S.; Butch, C. J.; Filimonov, S. N.; Ren, J. C.; Liu, W. Switchable Schottky Contacts: Simultaneously Enhanced Output Current and Reduced Leakage Current. *J. Am. Chem. Soc.* **2019**, *141*, 1628−1635.

(32) Heyd, J.; Scuseria, G. E.; Ernzerhof, M. Hybrid Functionals Based on a Screened Coulomb Potential. *J. Chem. Phys.* **2003**, *118*, 8207−8215.

(33) Grimme, S. Semiempirical GGA-type Density Functional Constructed with a Long-range Dispersion Correction. *J. Comput. Chem.* **2006**, *27*, 1787−1799.

(34) Dong, M. M.; He, C.; Zhang, W. X. Tunable Electronic Properties of Arsenene and Transition-Metal Dichalcogenide Heterostructures: A First-Principles Calculation. *J. Phys. Chem. C* **2017**, *121*, 22040−22048.

(35) Zhang, W. X.; He, W. H.; Zhao, J. W.; He, C. Electronic Properties of Blue Phosphorene/transition Metal Dichalcogenides van der Waals Heterostructures under in-plane Biaxial Strains. *J. Solid State Chem.* **2018**, *265*, 257−265.

(36) Debbichi, L.; Eriksson, O.; Lebegue, S. Two-Dimensional Indium Selenides Compounds: An Ab Initio Study. *J. Phys. Chem. Lett.* **2015**, *6*, 3098−3103.

(37) Lu, S.; Li, C.; Li, H. H.; Zhao, Y. F.; Gong, Y. Y.; Niu, L. Y.; Liu, X. J.; Wang, T. The Effects of Nonmetal Dopants on the Electronic, Optical and Chemical Performances of Monolayer g-C₃N₄ by First-principles Study. *Appl. Surf. Sci.* **2017**, *392*, 966−974.

(38) Peljhan, S.; Kokalj, A. Adsorption of Chlorine on Cu (111): A Density-Functional Theory Study. *J. Phys. Chem. C* **2009**, *113*, 14363−14376.

(39) Javaid, S.; Javed Akhtar, M. An ab-initio Density Functional Theory Investigation of Fullerene/Zn-phthalocyanine (C₆₀/ZnPc) Interface with Face-on Orientation. *J. Appl. Phys.* **2015**, *118*, 045305.

(40) Zhuang, H. L. L.; Hennig, R. G. Single-Layer Group-III Monochalcogenide Photocatalysts for Water Splitting. *Chem. Mater.* **2013**, *25*, 3232−3238.

(41) Yang, H. C.; Li, J. J.; Yu, L.; Huang, B. B.; Ma, Y. D.; Dai, Y. A Theoretical Study on the Electronic Properties of in-plane CdS/ZnSe Heterostructures: Type-II Band Alignment for Water Splitting. *J. Mater. Chem. A* **2018**, *6*, 4161−4166.

(42) Vante, N. A.; Jaegermann, W.; Tributsch, H.; Honle, W.; Yvon, K. Electrocatalysis of Oxygen Reduction by Chalcogenides Containing Mixed Transition Metal Clusters. *J. Am. Chem. Soc.* **1987**, *109*, 3251−3257.

(43) Dong, M. M.; He, C.; Zhang, W. X. A Tunable and Sizable Bandgap of a g-C₃N₄/graphene/g-C₃N₄ Sandwich Heterostructure: a van der Waals Density Functional Study. *J. Mater. Chem. C* **2017**, *5*, 3830−3837.